



ORIGINAL ARTICLE

Study of Gelatin-grafted-2-Acrylamido-2-methylpropane sulfonic acid hydrogels as a controlled release vehicle for amorphous solid dispersion of *Tripterygium Wilfordii* bioactive constituents



Abid Naeem^{a,b,\dag,*}, Chengqun Yu^{a,\dag}, Yali Liu^{b,c}, Yali Feng^a, Jinhui Fan^a, Yongmei Guan^a

^a Key Laboratory of Modern Preparation of Traditional Chinese Medicines, Ministry of Education, Jiangxi University of Chinese Medicine, 330004 Nanchang, China

^b Key Laboratory of Pharmacodynamics and Quality Evaluation on Anti-Inflammatory Chinese Herbs, Jiangxi Administration of Traditional Chinese Medicine, Nanchang Medical College, 1688 Meiling Road, Nanchang 330006, China

^c Key Laboratory of Pharmacodynamics and Safety Evaluation, Health Commission of Jiangxi Province, 1688 Meiling Road, Nanchang 330006, China

Received 13 March 2023; accepted 3 July 2023

Available online 8 July 2023

KEYWORDS

Hydrogels;
UHPLC-Q-TOF-MS;
Phytochemical;
Herbal medicine;
Free radical polymerization;
Anti-oxidants;
Antibacterial agents

Abstract The development of controlled-release preparations for herbal medicines remains challenging due to their complex compositions and distinct physicochemical properties. *Tripterygium Wilfordii* (TWHF) is a traditional Chinese medicine used to treat inflammatory diseases like rheumatoid arthritis, neurodegenerative and autoimmune diseases. The main active ingredients include diterpenes, triterpenes and alkaloids. These agents have poor pharmacokinetic and physicochemical characteristics, making it difficult to achieve therapeutic benefits. In the present study, a solid dispersion of TWHF (TWHF-SD) was prepared and loaded into Gelatin-grafted-2-Acrylamido-2-methylpropane sulfonic acid hydrogels (Gelatin-g-AMPS) for controlled drug release. A total of 48 compounds were identified in TWHF-SD using ultra-high performance liquid chromatography-quadrupole time-of-flight mass spectrometry (UHPLC-Q-TOF-MS) analysis.

* Corresponding author.

E-mail address: anaemk@ksu.edu.sa (A. Naeem).

^{\dag} These authors contributed equally to this work.

Peer review under responsibility of King Saud University.



Production and hosting by Elsevier

The hydrogel's structure and physicochemical properties were confirmed by scanning electron microscopy (SEM), Fourier-transform infrared spectroscopy (FTIR), X-ray diffraction (XRD), Thermogravimetric analysis (TGA), and Differential Scanning Calorimetry (DSC). Studies regarding hydrogel structure–function relationships were conducted, such as average weight between two or more crosslinks (Mc), polymer volume fraction (V_{2,s}), and diffusion coefficient (D). Hydrogel swelling and drug release from loaded hydrogels were slightly higher at pH 1.2 (swelling ratio of 60.84%, drug release of 85.08) than at pH 7.4 (swelling ratio of 46.46%, drug release of 75.03%) after 48 h. The gel fraction of hydrogel increased with increasing polymer/crosslinker ratios. Additionally, *in vitro* studies confirmed that the developed hydrogels were effective against bacterial growth and had good antioxidant properties.

© 2023 The Authors. Published by Elsevier B.V. on behalf of King Saud University. This is an open access article under the CC BY-NC-ND license (<http://creativecommons.org/licenses/by-nc-nd/4.0/>).

1. Introduction

Herbal medicines have been used for thousands of years to treat a wide range of diseases (Naeem et al., 2022a, 2022b, 2022c). However, due to the complexity of herbal medicines' compositions, there are very few dosage forms available (Sun et al., 2022). Herbal medicines are most often prepared as crude extracts, which can either be dried or not, containing both primary and secondary metabolites (Fan et al., 2022). The primary metabolites (PMs) of plants include amino acids, proteins, lipids, and sugars (Sheridan et al., 2015). While, secondary metabolites (SMs) are small molecules produced by plants having bioactive and non-bioactive properties.

The pharmacological effects of herbal extracts diminish or even disappear when many of the bioactive components are separated and purified. The therapeutic efficacy of herbal extracts has been observed to decrease due to the reduction in the pharmacokinetic synergy between active ingredients following the purification of herbal extracts (Li and Vederas 2009, Elfawal et al., 2015). Bioactive compounds in their pure form demonstrate poor pharmacokinetic properties when administered orally, compared to herbal extracts containing the same components (Naeem et al., 2022a, 2022b, 2022c). The pharmacological effects of herbal medicines are usually based on synergistic interactions between several components with diverse properties and activities (Weathers et al., 2011).

Many of the small molecules present in herbal extracts have the potential to assist in the solubilization of other bioactive substances which coexist with them in the extracts (Jürgenliemk and Nahrstedt 2003). Herbal extracts may become more water-soluble, but this does not necessarily indicate that all of the constituents have been dissolved (Zhao et al., 2020). The compounds seem to solubilize rather than becoming more soluble. For oral consumption, herbal extracts are usually prepared as powders that are reconstituted in water (Tchicailat-Landou et al., 2018). Since herbal extracts contain hydrophilic primary metabolites, powdered herbal extracts can be considered as an amorphous solid dispersion containing high concentrations of bioactive compounds (Williams et al., 2013, Taylor and Zhang 2016).

Tripterygium Wilfordii Hook F. (TWHF) exhibits anti-inflammatory, immunosuppressive, and anti-neoplastic properties. Several bioactive components are present in TWHF extracts, including terpenoids, glycosides, lignans, and alkaloids. The terpenoids present in TWHF include sesquiterpenes, diterpenes (tripdiolide, triptonide, and triptolide), and triterpe-

nes (wilforlide A and celastrol) (Liu et al., 2021). Triptolide is the most abundant and pharmacologically active of the metabolites detected in TWHF extracts. It inhibits tumors cell growth, glomerular sclerosis, fibrosis, and inflammation, as well as reduces oxidative stress (Tong et al., 2021). Celastrol has been extensively investigated as a potential treatment for autoimmune diseases, chronic inflammation, asthma, and neurological disorders and also shows inhibitory effects against various types of cancer cells (Lim et al., 2021). TWHF tablets are used to treat inflammatory and autoimmune diseases, such as rheumatoid arthritis, glomerular nephritis, nephrotic syndrome, and systemic lupus erythematosus (SLE) (Zhang et al., 2021). However, these tablets have to be taken orally three times per day, which is inconvenient for patients. In addition, it is associated with serious side effects, including nephrotoxicity and hepatotoxicity (Lin et al., 2021). Many sustained dosage forms, such as gastric floating tablets and multi-particulate time-controlled release capsules (MTRC), have been developed in order to improve compliance and reduce the toxicities associated with TWHF. However, tablets and pellets delivered by gastric floating may have limited sustained release. Other disadvantages include a complex preparation process and lack of industrial applications (Tang et al., 2019).

In recent decades, researchers around the globe have been developing advanced delivery systems to improve traditional medicinal agents in terms of their clinical safety, effectiveness, and ease of administration (Rahman et al., 2020). Controlled delivery systems are more effective than traditional dosage administration methods because they reduce side effects, decrease the dosage, and improve patient compliance with the treatment (Laffleur and Keckeis 2020). Hydrogels are three-dimensional (3D) water-swollen crosslinked hydrophilic networks that can withstand dissolution in water, as well as in biological fluids. Because hydrogels contain a high amount of water, which allows them to effectively simulate the natural tissue environment (Vigata et al., 2020). Water absorption in hydrogels is triggered by the presence of hydrophilic groups in the backbone of polymer chains, such as hydroxyl, amino, and carboxyl groups. Biologically, hydrophilic, biodegradable and chemically crosslinked hydrogels are stronger than their physically synthesized counterparts due to the interaction of naturally occurring polymers and synthetic polymers. One of the biggest advantages of hydrogels is their smoothness and flexibility, which helps to minimize inflammation in the surrounding tissues (Kesharwani et al., 2021). The porous hydrogel network structure facilitates the loading of drugs and the release of bioactive compounds. The porosity of the structure

is controlled by a number of factors, such as the attraction of the hydrogels to the aqueous conditions under which they have become swollen and the density of the crosslinking agents in the gel matrix. Thus, the porous hydrogel structure allows efficient loading of bioactive agents into the gel matrix and controlled release of the drugs based on the diffusion coefficients of small molecules and large molecules (Jacob et al., 2021).

Natural polymer gelatin is a fibrous protein obtained by hydrolyzing collagen in an alkaline or acidic solution. Its biodegradability, biocompatibility, non-immunogenicity, and commercial availability make gelatin a valuable biomedical ingredient (Mushtaq et al., 2022). Furthermore, its structure contains an arginine, glycine, and asparagine sequence that enhances the adhesion and migration of cells. Gelatin is capable of absorbing ten times more water than its mass. Pharmaceutical capsules contain gelatin, which melts above 30 °C and easily releases drugs into the digestive system. Additionally, gelatin's hydrophilic properties facilitate the permeation of body fluids into the particles, resulting in a greater release of drugs through diffusion (Salahuddin et al., 2021). 2-acrylamido-2-methylpropane sulfonic acid (AMPS) is a monomer that contains sulfonic acids, amides, and carbonyls, suitable for establishing hydrogel interconnections (Cheng et al., 2020). Ethylene glycol dimethacrylic acid (EGDMA) is generally used for chemical crosslinking of hydrogels (Kakkar and Narula 2022).

Based on the advantages of hydrogels for controlled drug delivery, we loaded TWHF-SD into hydrogels and characterized their physicochemical properties. Different pH-valued solutions of phosphate buffers (pH 1.2 and pH 7.4) were used to investigate swelling patterns and drug release mechanisms. Several techniques were employed in order to characterize the hydrogel, including thermal properties, compatibility between ingredients, sol-gel fractions, morphology, porosity, biodegradation, and mechanical characteristics. The effect of polymer and crosslinker concentrations on the swelling and release behavior of hydrogels was also investigated. Moreover, the TWHF-SD-loaded hydrogels were evaluated for antioxidant activities and antibacterial properties.

2. Materials and methods

2.1. Materials

Gelatin from Porcine skin (Gel; MW: 40,000 to 50,000 Da) was obtained from the Tianjin Fuchen chemical reagents factory, China. 2-Acrylamido-2-methyl-1-propanesulfonic acid (AMPS; MW: 207.25 g/mol), ammonium persulfate (APS), and ethylene glycol dimethacrylate (EGDMA; MW: 198.22 g/mol), were obtained from Sigma-Aldrich, Saint Louis, USA. Sodium bisulfite (SHS) was purchased from Shanghai Aladdin biochemical technology, China. ABTS, DPPH, and Cefepime (HCL) were procured from Meilune biological company (China). *Tripterygium Wilfordii* was acquired from Jiangxi Jiangzhong Traditional Chinese Medicine Co., Ltd., whose authenticity was certified by Prof. Deng Kezhong (School of Pharmacy, Jiangxi University of Chinese Medicine; voucher number: J20221014).

Bacterial strains such as *Staphylococcus aureus* (*S. aureus*: ATCC25923HBJZ005), *Pseudomonas aeruginosa* (*P. aeruginosa*: ATCC27853HBJZ017), and *Escherichia coli* (*E. coli*:

ATCC25922HBJZ087) were procured from Qingdao Hope Biotechnology, Co, Ltd., Shandong, China.

2.2. Preparation of TWHF-SD

TWHF (80 g) was added to ultra-pure water (800 mL) in an electric heating sleeve, soaked for 30 min, and then subjected to heated reflux extraction to obtain the extract. The extract was then filtered through a 200-mesh screen. The filtered extract was then concentrated by rotating vacuum evaporators (Xiamen Jingyi Xingye Technology Co., LTD). Firstly, the extract was refrigerated at -20 °C for 24 h, followed by lyophilization for 2–3 days (Ningbo Xinzhi Biotechnology Co., LTD) to obtain freeze-dried TWHF-SD (Guan et al., 2023). The total yield of the TWHF extracts powder obtained was 9.75%.

2.2.1. Qualitative determination of TWHF-SD using UHPLC-Q-TOF-MS

The samples were analyzed using the ACQUITY UPLC® BEH C18 column (2.1 × 100 mm, 1.8 μm) at a temperature of 30 °C (Sun et al., 2019). We eluted the column with a gradient of A (0.1% formic acid in purified water) and B (Acetonitrile) at a flow rate of 0.25 mL/min as follows: 0–18 min 5%–40% B; 18–55 min 40%~95% B; 55–57 min 95%~95% B; 57–57.1 min 95%–5% B; 57.1–60 min 5%~5% B. The volume of the injection was 1 μL. During the present study, data were collected using a Waters Xevo G2-S QT mass spectrometer equipped with a water electrospray ionization interface (Waters, USA), under both negative and positive ionization conditions. The time-of-flight mass spectrometry (TOF/MS) conditions were optimized as follows: the desolvation gas flow rate was 600 L/h; the desolvation temperature was 550 °C; the capillary voltage was 4.5–5 kV; the source temperature was 500 °C; the conical hole voltage was ±100 V; and the cone gas flow was 50 L/h. Mass spectrometers were programmed to scan over a range of 100–1500 *m/z*, with a collision energy of ±30 eV. The exact mass of components and fragment ions was determined using MassLynx 4.1 software.

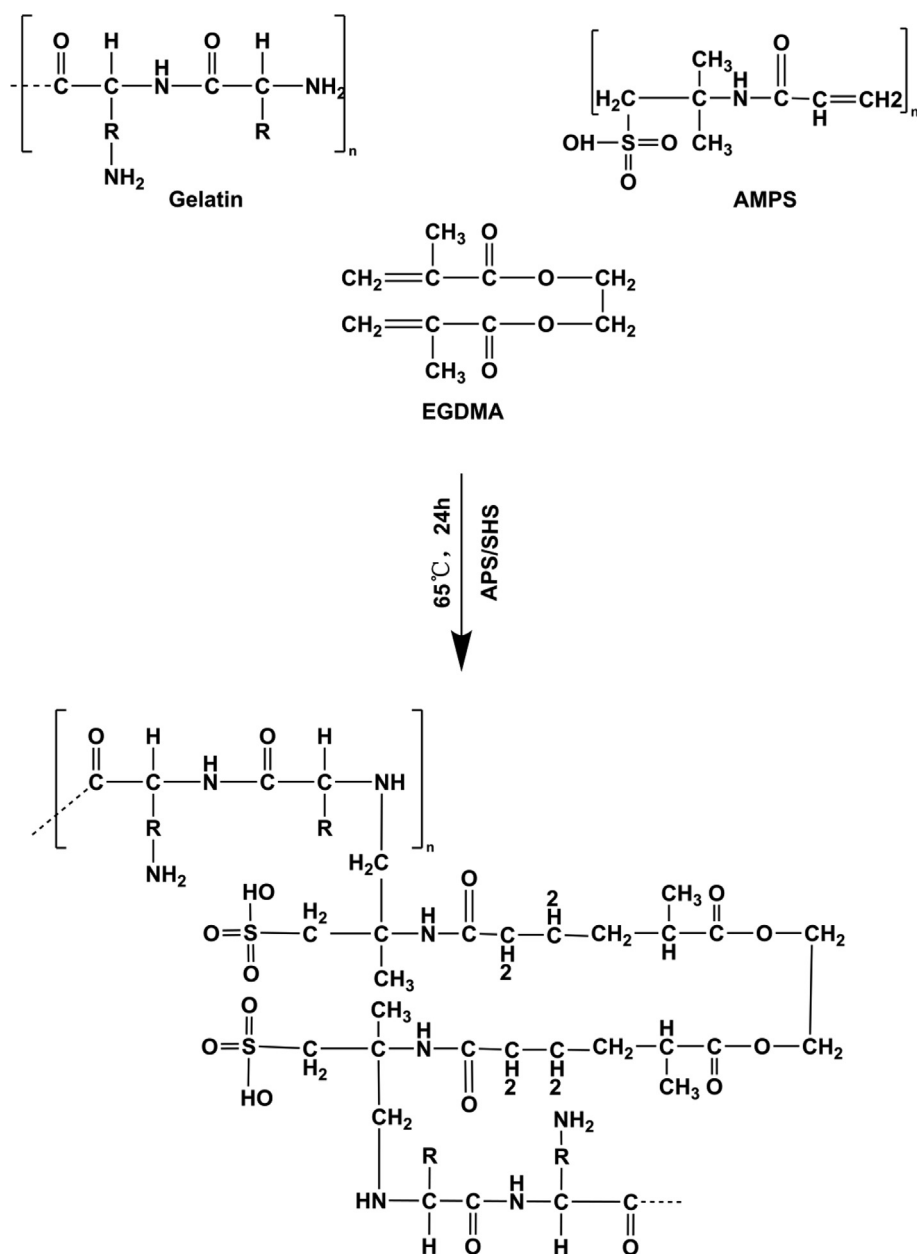
2.3. Fabrication of Gelatin-g-AMPS hydrogels

Free radical polymerization was used to prepare the hydrogels, with a few modifications (Zang et al., 2022). Briefly, specified quantities of gelatin, APS/SHS, AMPS and EGDMA were weighed carefully and placed in separate glass bottles for each formulation (Table 1). In each labelled vial, sufficient water was added and stirred continuously until a clear solution was obtained. Gelatin was continuously stirred at 50 °C to ensure its complete dissolution. These labelled solutions were then mixed according to the order in which they had been labelled. Briefly, APS/SHS was added to AMPS and mixed evenly before adding the gelatin, thereby eliminating any lumps in the mixture. After ultrasonication, the resulting homogeneous solution was bubbled with nitrogen for 30 min to remove bubbles. EGDMA was then introduced dropwise into the mixture as a final step. In the next step, the final solution was transferred to a 50 °C constant temperature water bath. The water bath temperature was gradually increased to 65 °C. After 24 h, the hydrogels were formed and cut into 8 mm discs and vacuum dried for a week at 40 °C. Fig. 1 presents a proposed

Table 1 Composition of Gelatin-g-AMPS hydrogel formulations.

Formulation	Gelatin (g)	APS/SHS (g)	AMPS (g)	EGDMA (g)
GAE-1	0.5	0.3/0.3	20	0.5
GAE-2	0.5	0.3/0.3	20	1
GAE-3	0.5	0.3/0.3	20	1.5
GAE-4	0.5	0.3/0.3	12	1
GAE-5	0.5	0.3/0.3	20	1
GAE-6	0.5	0.3/0.3	28	1
GAE-7	0.3	0.3/0.3	20	1
GAE-8	0.5	0.3/0.3	20	1
GAE-9	0.7	0.3/0.3	20	1

Note: Bold letters signify higher feeding amounts of components.

**Fig. 1** The proposed chemical structure of Gelatin-g-AMPS hydrogels.

chemical structure of the synthesized Gelatin-g-AMPS hydrogel.

2.4. TWHF-SD loading in hydrogels

A swelling-diffusion technique was used to load TWHF-SD into Gelatin-g-AMPS hydrogels (Yu et al., 2022). Briefly, TWHF-SD was dissolved in pH 7.4 buffer, and a 1% solution of it was prepared, and then pre-weighed dried hydrogel was soaked in the solution for three days while being stirred slowly. After three days, the hydrogel discs were removed from the solution, dried completely, and weighed. The amount of TWHF-SD-loaded hydrogel was then determined by the weight subtraction method. Additionally, the TWHF-SD loading was confirmed by extracting all the TWHF with water and analyzing it using ultraviolet spectrometry (wavelength of 271 nm).

$$\text{TWHF-SD loading} = \text{TWHF-SD loaded hydrogel} - \text{Unloaded hydrogel} \quad (1)$$

2.5. Solid-state characterization of hydrogels

2.5.1. Fourier transform infrared spectroscopy (FTIR)

FTIR spectra of pure gelatin, TWHF-SD, AMPS, EGDMA, and unloaded and drug loaded hydrogel discs were determined (Tang et al., 2022). The FTIR spectrophotometer (Perkin Elmer, UK) was used to analyze the samples in the scanning range of 400 and 4000 cm^{-1} .

2.5.2. Thermal analysis

The samples were subjected to thermal analysis, including thermogravimetric analysis (TGA) using Exstar TG/DTA6300TG (SHI Nano, Japan), and differential scanning calorimetry (DSC) manufactured by Perkin Elmer (UK) (Martinez-Serrano et al., 2022). The dried hydrogel discs were passed through sieve no.40 in order to attain the preferred particle size of the hydrogel. We placed 0.5–5 mg of the sample in an aluminum pan connected to a microbalance. The samples were all examined under nitrogen gas (10 mL/min) and heated at a rate of 10 $^{\circ}\text{C}/\text{min}$.

2.5.3. X-ray diffraction (XRD)

X-ray diffractograms were obtained using a powder X-ray diffractometer (TD-3500 X-ray diffractometer, China) (Sousa et al., 2023). Glass slides were used to level the sample surface after being inserted into the sample holder. The samples were analyzed at 2θ (10° – 60°) at a speed of $2^{\circ} 2\theta/\text{min}$ with a copper ray source of 30 kV and 20 mA to observe the samples. The analyzed samples included gelatin, TWHF-SD, AMPS, and drug-loaded and unloaded hydrogels.

2.5.4. Morphological analysis

Hydrogel surface morphology was analyzed with a scanning electron microscope (Quanta 250, FEI, Czech Republic) (Kocak et al., 2022). Double-sided tape was used to attach dried hydrogels to an aluminum stab for fixation. The gold coating was conducted in a highly vacuumed evaporator fitted with a thick gold lining.

2.5.5. Mechanical properties evaluation

We assessed each formulation's mechanical properties using a TA.XT plus texture analyzer (Stable Micro Systems, UK) with a stainless-steel cylindrical probe (P/5S) at a speed of 1 mm per second. These mechanical properties include tensile strength (TS, N/mm) as well as elongation at break (EAB, %) (Li et al., 2022). The probe's force and displacement were measured during the puncture of the hydrogels to determine TS and EAB.

$$TS = \frac{F_m}{T_h} \quad (2)$$

$$EAB = \frac{\sqrt{D^2 + R^2}}{R} - 1 \quad (3)$$

The maximum force is F_m , and the thickness is T_h . Probe displacement from initial contact to breaking of the hydrogel is D , and the orifice plate radius is R .

2.5.6. Sol-gel fraction determination

The Soxhlet extraction procedure was used in order to evaluate the insoluble, uncrosslinked, and crosslinked material components of the synthesized hydrogel. The sol component of a hydrogel is soluble, while the gel component is insoluble. The hydrogel disc was maintained at 85 $^{\circ}\text{C}$ for around eight hours in a round-bottom flask containing water and connected to a condensation unit. A vacuum oven was used to dry the hydrogel completely after removal. Sol-gel fractions were calculated using the following equations (Ghumman et al., 2022).

$$\text{Sol fraction \%} = \frac{X_1 - X_2}{X_2} \times 100 \quad (4)$$

$$\text{Gel fraction} = 100 - \text{sol fraction} \quad (5)$$

Whereas, X_1 refers to the weight of the sample before extraction. And the constant weight for the hydrogel after extraction is denoted by X_2 .

2.5.7. Porosity of hydrogels

Hydrogel porosity was evaluated and analyzed using a solvent replacement method. Dried hydrogel discs (K_1) were accurately weighed and submerged in pure ethanol for five days. The hydrogel discs were then gently blotted with filter paper so that any excess solvent could be removed and reweighed (K_2). We measured the discs' thickness and diameter as well. According to the following equation, porosity was determined (Chang et al., 2022).

$$\text{Porosity percentage (\%)} = \frac{K_2 - K_1}{\rho v} \times 100 \quad (6)$$

Whereas, absolute ethanol density is represented by ρ and swollen hydrogel volume by v .

2.5.8. Swelling behaviour evaluation

The equilibrium-swelling ratio (ESR) of the prepared formulations was determined by performing water uptake test at pH 1.2 and 7.4 (Jozaghkar et al., 2022). Hydrogel discs were weighed thoroughly before being placed in pH media, which were weighed periodically after being blotted with filter paper. We repeated the process until an equilibrium weight was achieved. Three readings were taken in order to verify the weight achieved. Dynamic swelling was determined using the equation shown below:

$$ESR = \frac{Y_t - Y_i}{Y_i} \times 100 \quad (7)$$

The weight at time t is denoted by Y_t , and the initial weight of the hydrogel is indicated by ' Y_i '.

2.5.9. In vitro dissolution and drug release kinetics

In vitro dissolution analysis of fabricated hydrogels was conducted on USP dissolution equipment type II to estimate the optimal media for the substantial release of drug molecules (Qu et al., 2019). *In vitro* dissolution analysis was carried out using buffer solutions (900 mL) with pH 1.2 and 7.4 at 37 °C. At a predetermined interval, the same volume of fresh medium was added after each 5-mL aliquot. A UV spectrophotometer (T6 New Century; Beijing GM) was used to observe the release of TWHF at a wavelength of 271 nm (maximum absorption wavelength).

$$Drug\ release\% = \frac{(\text{Amount of released drug})}{(\text{Amount of loaded drug})} \times 100 \quad (8)$$

Hydrogel dissolution results were analyzed using different kinetic models, including first-order, zero-order, Korsmeyer-Peppas, and Higuchi models in order to determine the drug release mechanism.

2.6. Hydrogel polymer network variables

Hydrogel structures and properties can be analyzed using the following major indicators (Singh and Singh 2020).

2.6.1. Diffusion coefficient

Diffusion coefficient estimation was performed using the following formula.

$$D = \pi \left(\frac{h \cdot \theta}{4 \cdot q_{eq}} \right)^2 \quad (9)$$

Where, q_{eq} indicates equilibrium swelling of a hydrogel disc, and h refers to its thickness.

2.6.2. Volume fraction of polymer ($V_{2,s}$)

The $V_{2,s}$ values were calculated using the equation below.

$$V_{2,s} = \frac{1}{V_{eq}} \quad (10)$$

2.6.3. Molecular weight distribution between crosslinks (Mc)

Mc measures the degree of crosslinking in polymer networks. The following equation can be used to determine it.

$$Mc = \frac{dp \cdot V_s \left(v^{\frac{1}{2}} \cdot V_{2,s} - V_{2,s} / 2 \right)}{\ln(1 - V_{2,s}) + V_{2,s} + \chi V_{2,s}^2} \quad (11)$$

Here, dp indicates polymer density. V_s represents the solvent volume, and χ is the Flory-Huggins polymer-solvent interaction parameter.

2.6.4. Solvent interaction variables calculation (χ)

Solvent interaction factors (χ) can be calculated using the Flory-Huggins theory.

$$\chi = \frac{\ln(1 - V_{2,s}) + V_{2,s}}{V_{2,s}^2} \quad (12)$$

Whereas, $V_{2,s}$ is a measure of the volume fraction of the swollen gel.

2.6.5. Repetition rate of intercrosslinks (N)

N was calculated using Mc data. We calculated the number of repeating units and crosslinks using the following equation.

$$N = \frac{2Mc}{Mr} \quad (13)$$

Mr is the molar mass of the unit of repetition. This value is determined by the following formula:

$$Mr = \frac{m_{Gel} + m_{MGel} + m_{AMPS} + m_{MAMPS} + m_{EGDMA} + m_{EGDMA}}{m_{Gel} + m_{AMPS} + m_{EGDMA}} \quad (14)$$

Where m is the mass, while M is the molar mass of the hydrogel components.

2.7. Biodegradation analysis

The biodegradation of hydrogels was assessed in a 7.4 pH phosphate buffer solution at 37 °C ± 0.5 °C. Specifically, weighed discs of dry hydrogel were immersed over a period of time in a buffer solution with a pH of 7.4. These discs were then dehydrated in a vacuum oven at 40 °C, weighed again, and placed in a buffer solution with a pH of 7.4. The procedure was repeated for a week. For the calculation of hydrogel degradation, the following equation was used (Tapdiqov et al., 2022).

$$D = \frac{C_1 - C_2}{C_1} \quad (15)$$

D stands for degradation, C_1 stands for dry weight, and C_2 stands for the weight of the sample after immersion at a specific time (t).

2.8. Antioxidant activities determination

2.8.1. DPPH activity

The antioxidant activity of hydrogels was evaluated using the DPPH free radical scavenging assay. For this experiment, each sample was soaked in a specified amount of methanol for 24 h at ambient temperature in the dark. A DPPH-methanol solution (0.1 mM) was then mixed with the hydrogel extract solution. The mixture was vigorously shaken and then stored in a dark place for 30 min. The DPPH scavenging activity (DPPH %) was calculated based on the absorbance at 517 nm measured with a UV-Vis spectrophotometer (Xu et al., 2022).

$$DPPH(\%) = \frac{A_0 - A}{A_0} \times 100 \quad (16)$$

Whereas, sample extract absorbance is represented by A , whereas control absorbance is represented by A_0 .

2.8.2. ABTS assay

The TWHF-SD-loaded hydrogel was tested for radical scavenging activity using the ABTS assay. ABTS was radicalized by mixing 7.4 mM ABTS with 2.4 mM potassium persulfate solution overnight at room temperature. After the hydrogels were soaked in the ABTS solution, they were incubated at 37 °C for 30 min. At 730 nm, the absorbance was measured. The scavenging effect of ABTS was calculated based on the following formula (Lorz et al., 2019).

$$ABTS\ scavenging\ effect(\%) = \frac{A_0 - A_1}{A_0} \times 100 \quad (17)$$

The absorbance of ABTS is A_0 , while that of the sample is A_1 .

2.9. Antibacterial assessment

TWHF-SD-loaded hydrogels were tested against *Staphylococcus aureus*, *Pseudomonas aeruginosa*, and *Escherichia coli* using the disk diffusion method. Each bacterial suspension with a cell density of approximately 3×10^8 CFU·mL⁻¹ was cultured on an agar medium. Hydrogel samples were cut into small pieces and sterilized to prevent microbial contamination. Each hydrogel was then placed on cultured agar plates and incubated at 37 °C for 24 h. The bacterial inhibition zones were then determined (Abbasi et al., 2020).

$$\text{Percentage inhibition} = \frac{\text{Zone of inhibition of test sample (mm)}}{\text{Zone of inhibition of standard drug (mm)}} \times 100 \quad (18)$$

2.10. Statistical analysis

Data were expressed as mean \pm standard deviation. The statistical difference between adjacent data was determined using two-way ANOVA and Tukey's post-hoc test. The significance of the difference was determined using p-values of $p < 0.05$, $*p < 0.01$, and $***p < 0.001$.

3. Results and discussion

3.1. Identifying chemical constituents in TWHF-SD using UHPLC-Q-TOF-MS

The chromatograms in Fig. 2 depict the base peak intensities of the sample in both positive and negative ion modes. The identification of the major chemical components of TWHF was carried out using mass spectrometry software (MassLynx v4.1). Table 2 presents 48 chemical compounds identified from the results of MS and MS/MS analyses, reference literature, and relevant scientific literature. Most of these compounds are diterpenes, triterpenes, and alkaloids. It has been demonstrated that these ingredients possess a variety of biological properties and are often used to treat conditions such as rheumatoid arthritis, lupus erythematosus, and other autoimmune diseases. According to some studies, these components are responsible for the primary therapeutic effects of TWHF.

3.2. FTIR spectroscopy

FTIR spectra of gelatin, AMPS, EGDMA, TWHF-SD, unloaded, and TWHF-SD loaded hydrogels are shown in Fig. 3. In the infrared spectrum of TWHF-SD, the band at 3463 cm⁻¹ belongs to the -OH stretching vibration, the band at 2940 cm⁻¹ and 2846 cm⁻¹ belongs to the C-H stretching vibration, and the band at 1607 cm⁻¹ belongs to the C-C stretching vibration above the benzene ring (Chen et al., 2014). In the infrared spectrum of gelatin, the band at 1630 cm⁻¹ corresponds to the absorption band of C = O, 1525 cm⁻¹ corresponds to C-N stretching vibration and 1239 cm⁻¹ corresponds to the N-H bending vibration, and these findings are consistent with those of other researchers (Aguilar-Méndez et al., 2020). Based on the FTIR spectrum of AMPS, a band was observed at 1461 cm⁻¹ associated with the binding vibration of CH₂. The band at 1360 cm⁻¹ represents the -C-O stretching vibration, whereas 2981 cm⁻¹ reflects

the -CH stretching of -CH₂, and 1230 cm⁻¹ reflect the symmetrical stretching of the S = O functional group. FTIR spectrum of EGDMA revealed a band at 1713 cm⁻¹, indicative of stretching vibrations of C = O, along with bands at 1633, 1291 and 1153 cm⁻¹ corresponding to C = C and C-O stretching vibrations in both symmetric and asymmetric esters. Unloaded hydrogels display a different spectrum than their parent components. The band at 1458 cm⁻¹ is attributed to the -CH₂ binding vibration in AMPS. The band at 1630 cm⁻¹ is associated with the absorption band of C = O in gelatin. These bands and functional groups indicate that the polymers were successfully cross-linked. Additionally, FTIR analysis of TWHF-SD-loaded hydrogels was performed to confirm the presence of the TWHF-SD. The bands at 1453 cm⁻¹ and 1610 cm⁻¹ are representative of the TWHF-SD spectrum. The appearance of these functional bands of TWHF-SD demonstrated that TWHF-SD was successfully incorporated into the hydrogel.

3.3. TGA study

TGA was performed in order to assess the thermal integrity of all reagents and hydrogel systems (Fig. 4). Gelatin thermogravimetry results can be divided into three general stages. First, there is a weight loss of 5.8% between 30 and 95 °C, which may be attributed to water loss. The weight loss in the second stage reached 34.66% at 265–324 °C, which was attributed to gelatin degradation. In the 320–540 °C range, the weight loss was 69.25% due to residual material combustion (Ullah et al., 2019). TGA analysis of AMPS revealed a 6% weight loss at 208 °C and a further 20% between 210 and 250 °C, indicating AMPS dehydration. Furthermore, the sulfonic acid group began to decompose at 340 °C, and a weight loss of further 20% was observed within a temperature range of 250 to 340 °C (Naeem et al., 2023). TGA analysis of TWHF-loaded hydrogels revealed that an initial weight loss of 18% was caused by dehydration at 30 to 183 °C, followed by a 45% weight loss due to bond breakage between polymers at 183 to 331 °C. A gradual degradation of the polymer network occurred at 331 °C and continued until the polymer skeleton was completely degraded. The initial weight loss of 17% in the unloaded gel was caused by dehydration in the temperature range of 30–342 °C, followed by a 19% weight loss due to the breaking of bonds between the polymers in the temperature range of 342–367 °C. The polymer network began to decompose gradually after 367 °C and continued until the polymer backbone was fully decomposed. Based on the thermal profile of hydrogels with high residual weight, it can be concluded that the polymeric matrix provides greater stability against thermal degradation over a wide temperature range. The developed hydrogel also exhibits a slower weight loss rate as a result of stronger interaction between the polymer and monomer, as compared to the individual reactants. The development of rigid networks as well as the shifting of endothermic peak temperatures, can be attributed to a higher level of thermal stability (Liu et al., 2023a, 2023b).

3.4. DSC study

Gelatin showed a strong endothermic peak at 119.62 °C in the DSC analysis, which is consistent with previous studies

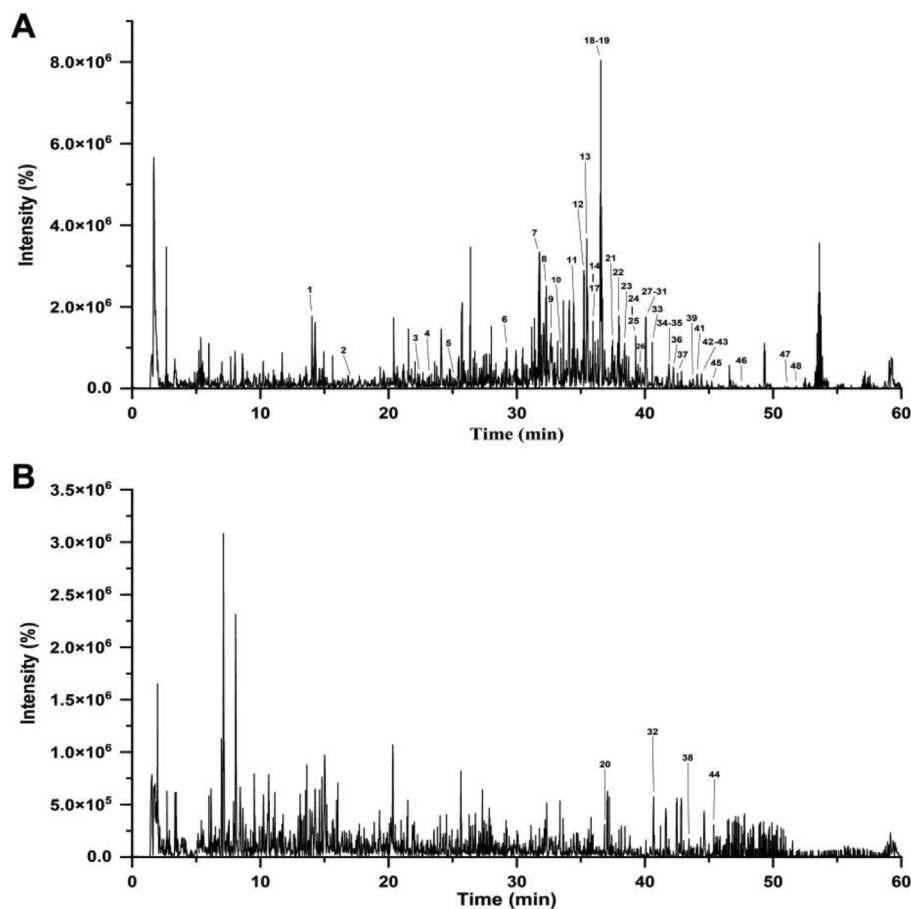


Fig. 2 TWHF-SD chromatograms obtained using UHPLC-Q-TOF-MS in positive (A) and negative ionization modes (B).

(Rahman et al., 2008). A DSC analysis of TWHF-SD revealed that there was a large endothermic peak at 81.02 °C, which was similar to the results obtained by other researchers. The AMPS analysis revealed an endothermic peak at 202 °C, indicating dehydration. One exothermic peak was observed around 315 °C in the developed hydrogel. Hydrogels at these temperatures exhibit exothermic peaks, indicating cross-linking of polymers which provides thermal stability to the newly formed network (Fig. 5). DSC analysis of synthesized hydrogels indicates that the formulations are more compatible with each other and form rigid networks by forming greater hydrogen bonds between the molecules indicating increased compatibility among the components. Therefore, the developed polymeric network is more thermally stable.

3.5. XRD studies

XRD analysis confirmed the physical state of TWHF-SD, gelatin, and the developed hydrogels, as shown in Fig. 6. The diffraction pattern of gelatin exhibited an extensive broadening peak between 15.0 and 25.0°, resulting from its α -helix and triple-helical structure (Shi et al., 2018). The XRD diffractogram of unloaded hydrogel exhibits a broader peak at $2\theta = 21.32^\circ$, indicating that the formulation is amorphous. Similarly, TWHF-SD shows a broader amorphous peak at $2\theta = 21.22^\circ$. The diffractogram of TWHF-SD loaded hydrogels,

however, shows a wider peak at $2\theta = 21.12^\circ$; however, no other intense peak of TWHF was observed at its respective region, possibly due to physical interactions between TWHF and polymeric network.

3.6. Morphological studies

Fig. 7 demonstrates that the hydrogels exhibited porous and compact surfaces that were somewhat coarse in texture. This morphological structure may indicate successful crosslinking between polymers and monomers. These properties are observed in hydrogels designed for biomedical purposes (Gu et al., 2020). The porous surface of the hydrogel allows water to penetrate directly into the spaces and fluid to diffuse within the network, thereby enhancing swelling characteristics. In addition, these pores allow drugs to attach to the surface or load inside the hydrogels and are released at the site where they are needed. The hydrogel can absorb aqueous fluid in large quantities through these pores. The durability of the hydrogel system depends on its solid mass and smooth surface. The microstructure of the hydrogel before and after drug loading was analyzed by scanning electron microscopy. Compared with the unloaded hydrogel, the surface of the drug-loaded hydrogels showed a porous structure with the drug attached to the surface and loaded inside the hydrogel through the porous network.

Table 2 Identification of main chemical components in TWHF-SD using UHPLC-Q-TOF-MS.

Peak No	Retention time/min	Compounds	Formula	Experimental m/z	Theoretical m/z	Error (ppm)	Mode
1	14.05	Celafurine	C ₂₁ H ₂₇ O ₃ N ₃	370.21284	370.21252	0.9	+
2	17.19	Celabenzine	C ₂₃ H ₂₉ O ₂ N ₃	380.23301	380.23325	-0.7	+
3	22.37	Celacinnine	C ₂₅ H ₃₁ O ₂ N ₃	406.249	406.2489	0.2	+
4	23.18	Tripterygiumine T	C ₃₂ H ₃₉ NO ₁₆	694.23403	694.23416	-0.2	+
5	25.13	Triptolide	C ₂₀ H ₂₄ O ₆	361.16329	361.16457	-2.1	+
6	29.19	Triptoquinone C	C ₂₀ H ₂₈ O ₄	333.20624	333.20604	0.6	+
7	31.99	Wilfordinine G	C ₃₆ H ₄₃ NO ₁₈	778.25592	778.25529	0.3	+
8	32.33	Alatusinine	C ₃₈ H ₄₇ O ₁₉ N	822.282	822.28151	0.6	+
9	32.36	Wilfordinine B	C ₃₈ H ₄₇ NO ₁₉	822.282	822.28151	0.6	+
10	33.50	Wilfordconine	C ₃₉ H ₄₅ NO ₁₉	832.26668	832.26586	1	+
11	34.55	Evonymine	C ₃₉ H ₄₉ NO ₁₈	820.30247	820.30224	0.3	+
12	35.29	Wilformic acid E	C ₃₀ H ₄₆ O ₅	487.34214	487.3418	0.7	+
13	35.48	Neotripterifordin	C ₂₀ H ₃₀ O ₃	319.22694	319.22677	0.5	+
14	35.60	Doianoterpene	C ₂₀ H ₂₈ O ₂	301.21606	301.21621	-0.5	+
15	35.63	1-deacetylwilfordine	C ₄₁ H ₄₇ NO ₁₈	842.28647	842.28659	-0.1	+
16	36.41	Tripterygiu mine W	C ₄₄ H ₄₇ NO ₁₈	878.28726	878.28659	0.8	+
17	36.44	Wilfordconine	C ₄₁ H ₄₇ O ₂₀ N	874.27718	874.27642	0.9	+
18	36.53	9'-O-acetyl-7-deacetox y-7-oxowilfortrine	C ₄₁ H ₄₅ NO ₂₀	872.26143	872.26077	0.8	+
19	36.56	Wilfordinine E	C ₃₈ H ₄₇ O ₁₈ N	806.28678	806.28659	0.2	+
20	36.77	23-nor-6-oxe-demethy L-pristimerol	C ₂₈ H ₃₆ O ₅	451.24915	451.249	0.3	-
21	37.61	Ent-19-hydroxykaur-16-ene	C ₂₀ H ₃₀ O ₂	303.2319	303.23186	0.1	+
22	38.32	Cangoronine	C ₃₀ H ₄₄ O ₅	485.3258	485.32615	-0.7	+
23	38.42	Triptoquinone B	C ₂₀ H ₂₆ O ₄	331.19078	331.19039	1.2	+
24	39.10	Linoleic acid	C ₁₈ H ₃₂ O ₂	281.24773	281.24751	0.8	+
25	39.20	Wilformine D	C ₄₃ H ₄₉ NO ₂₁	916.28776	916.28698	0.8	+
26	39.60	Tripterinin	C ₂₀ H ₃₀ O ₄	335.22188	335.22169	0.6	+
27	40.10	Triptonoditerpenic acid	C ₂₁ H ₂₈ O ₄	345.20637	345.20604	1	+
28	40.10	Triptobenzene D	C ₂₀ H ₂₆ O ₂	299.20061	299.20056	0.2	+
29	40.17	Wilforgine	C ₄₁ H ₄₇ NO ₁₉	858.28218	858.28151	0.8	+
30	40.24	Wilforgine	C ₄₁ H ₄₇ O ₁₉ N	858.28218	858.28151	0.8	+
31	40.28	Triptonine B	C ₄₆ H ₄₉ NO ₂₂	968.28282	968.2819	1	+
32	40.47	Triptophenolide	C ₂₀ H ₂₄ O ₃	311.16595	311.16527	2.2	-
33	40.88	Triptonolide	C ₂₀ H ₂₂ O ₄	327.15941	327.15909	1	+
34	41.95	Wilforline A	C ₃₀ H ₄₆ O ₃	455.35203	455.35197	0.1	+
35	41.98	Triptotrimeric acid C	C ₃₀ H ₄₈ O ₄	473.36263	473.36254	0.2	+
36	42.26	19-hydroxy-7-oxo-18 (4 → 3) abeo-abieta-3,8,11,13-tetraen-18-oic acid lactone	C ₂₀ H ₂₂ O ₃	311.16439	311.16417	0.7	+
37	42.39	Hyponine E	C ₄₅ H ₄₈ N ₂ O ₁₉	921.29294	921.2924	0.6	+
38	43.67	Tingenin B	C ₂₈ H ₃₆ O ₄	435.25393	435.25408	-0.4	-
39	43.82	Triptonoterpene methyl ether	C ₂₁ H ₃₀ O ₃	331.22666	331.22677	-0.3	+
40	44.07	2α,3β,-dihydroxy-olean-12-ene-22,29-lactone	C ₃₀ H ₄₆ O ₄	471.34698	471.34689	0.2	+
41	44.07	Wilforlide B	C ₃₀ H ₄₄ O ₃	453.33643	453.33632	0.2	+
42	44.48	Congorinine E-I	C ₄₃ H ₄₉ O ₁₈ N	868.3022	868.30224	0	+
43	44.48	Wilforine	C ₄₃ H ₄₉ NO ₁₈	868.3022	868.30224	0	+
44	45.11	Regeol A	C ₂₈ H ₄₀ O ₄	439.28565	439.28538	0.6	-
45	45.29	Triptocalline A	C ₂₈ H ₄₂ O ₄	443.31565	443.31559	0.1	+
46	47.34	Orthosphenic acid	C ₃₀ H ₄₈ O ₅	489.35724	489.35745	-0.4	+
47	51.14	3β,28-dihydroxy-3-oxo-olean-12-en-29-oic acid	C ₂₉ H ₄₄ O ₄	457.33119	457.33124	-0.1	+
48	51.32	Celastrol	C ₂₉ H ₃₈ O ₄	451.28462	451.28429	0.7	+

3.7. Mechanical properties of hydrogels

Hydrogels should be tested for their mechanical properties, including tensile strength (TS) and elongation at break (EAB), before they can be used for biomedical applications. The mechanical properties of the hydrogel gradually improved as the concentration of the gelatin was increased, and our results are consistent with those of other researchers (Table 3) (Biswal et al., 2016). AMPS is an anionic monomer, which results in a decrease in the mechanical strength of the hydrogel

which may be attributed to an increase in electrostatic repulsion and osmotic pressure. The tensile strength also increased as the EGDMA content increased.

3.8. Sol-gel studies

Hydrogels are obtained through the polymerization of crosslinkers, monomers, and polymers. "Sol fractions" are non-crosslinked portions of hydrogels, while "gel fractions" are crosslinked portions of hydrogels. The lack of reactive sites

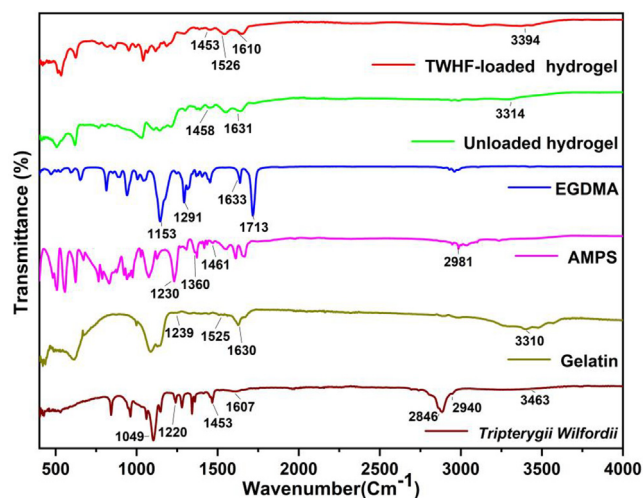


Fig. 3 FTIR spectra of TWHF-SD, gelatin, AMPS, EGDMA, unloaded and TWHF-SD-loaded hydrogels.

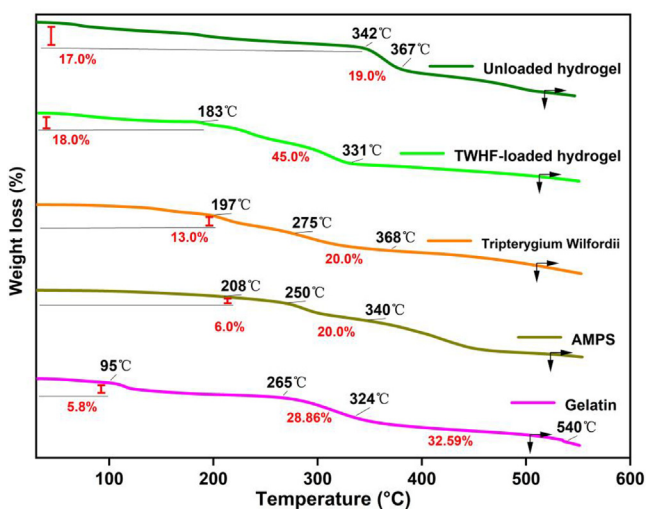


Fig. 4 TGA thermograms of gelatin, AMPS, TWHF-SD, EGDMA, unloaded and TWHF-loaded hydrogels.

during the polymerization process of hydrogels results in uncrosslinking of some parts (sol fraction) in the case of a large number of single or multiple ingredients being used. Thus, the crosslinking percentage of the hydrogel must be determined (Naeem et al., 2022a, 2022b, 2022c). The sol-gel properties of all hydrogel formulations were tested (Fig. 8A, B, and C). Sol-gel evaluation is principally used to assess the degree of uncrosslinking among polymers within a system. Depending on the material ratio in the hydrogel formulations, the gel fraction percentage ranges from 80.50% to 96.30%. The increase in gelatin concentration may result in a gradual increase in gel fraction, possibly due to the increase in biopolymer concentration. The findings of this study are in agreement with those of other researchers (Tytgat et al., 2018). Additionally, since AMPS are hydrophilic monomers, they allow more room for chemical reactions to take place. As AMPS concentration increases, the gel fraction increases. Gel fractions increase when the amount of EGDMA in the hydrogel increases, as

EGDMA contributes to their formation as a result of its crosslinking properties.

3.9. Porosity study

The porosity of hydrogels influences several of their properties, including swelling, loading, and release of drugs. Pore size affects swelling, which contributes to greater loading and release of drugs. The high viscosity of the reaction mixture results in a higher porosity, inhibiting the egress of bubbles. As a result, the material becomes porous due to a large number of interconnected channels. Porosity percentages varied from 41.81% to 91.62% at different reagent ratios. Gradually, the porosity of the hydrogel increased with an increase in the gelatin ratio. SEM images of the newly synthesized hydrogel show that it has rough and porous properties, which is consistent with other researchers' findings (Elblbesy et al., 2020). EGDMA leads to the formation of tight junctions and cross-linked bulk densities, resulting in a decrease in porosity. A higher concentration of AMPS increases porosity since the sulfonate groups generate more electrostatic forces. AMPS contains a hydrophobic alkyl group, which can reduce hydrogen bond interactions by forming microregions of hydrophobicity. So, in the hydrogel preparation, the pores and network sizes are enhanced, which agrees with other studies (Khan et al., 2022).

3.10. Biodegradation studies

Fig. 9 depicts the results of a biodegradation experiment conducted on the prepared hydrogel to determine its degradation rate. Biodegradation studies were conducted in order to determine the degradation rate of the hydrogel prepared at various material ratios. Different weight ratios will likely have a significant impact on the degradation rate of the hydrogel. Hydrogels of different proportions showed varying rates of degradation between 5.6% and 9.3%. There was a positive correlation between the amount of gelatin and the rate of weight loss of the composite hydrogel (Hu et al., 2011). It was found that as the EGDMA ratio increased in the material, the degradation speed of hydrogels slowed down. It may be due to the generation of functional groups, which resulted in the production of a large number of free radicals. In addition to strengthening hydrogel crosslinks, these free radicals also play a significant role in the polymerization reaction, which slows down the degradation process.

3.11. Hydrogel network properties

A number of structural parameters, including the average molecular weight between crosslinks M_c (degree to which the polymer has been crosslinked), the polymer volume fraction $V_{2,s}$ (the amount of fluid absorbed and retained by the network), the solvent interaction parameter χ , and the number of repeats between crosslinks N , were calculated for the synthesized hydrogels. The values of various structural parameters are shown in Table 4. These parameters are important for hydrogels because they indicate the compatibility of the solvent with the polymers and, thus, the maximum capacity for uptake and holding. $V_{2,s}$ and χ values increased as EGDMA concentration was increased, suggesting that hydrogel struc-

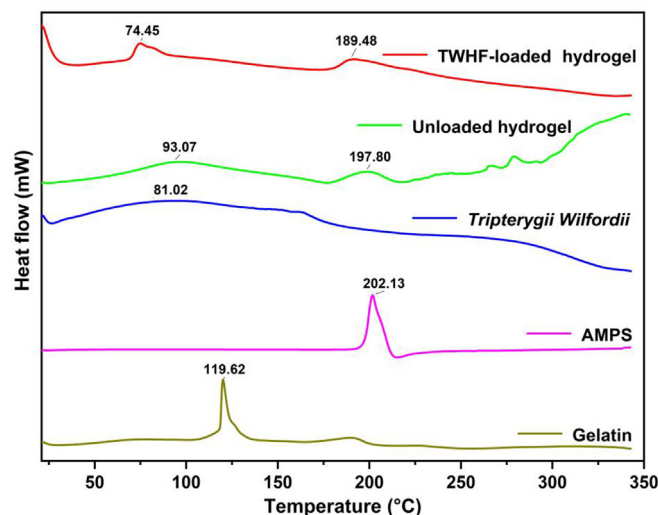


Fig. 5 DSC thermogram of gelatin, AMPS, TWHF-SD, unloaded and TWHF-loaded hydrogels.

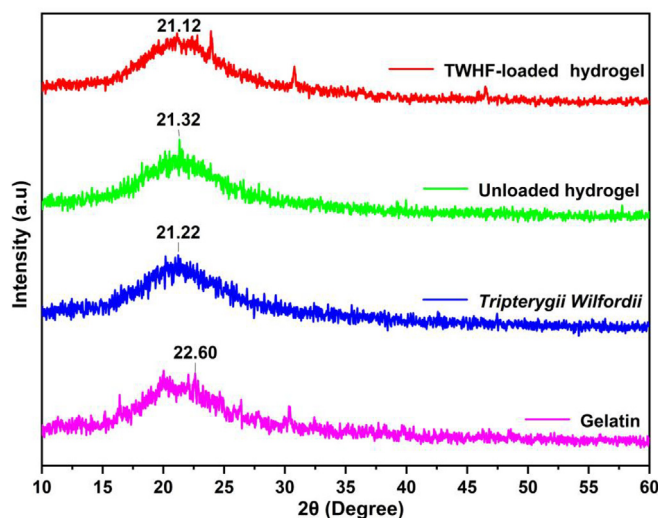


Fig. 6 XRD patterns of gelatin, TWHF-SD, unloaded and TWHF-loaded hydrogels.

tures became tighter and stiffer, consistent with other studies (Jalil et al., 2017). Mc and N values also decreased with an increase in the concentration of EGDMA. The decrease in Mc and N values is due to the increased crosslinking density caused by the increasing amount of EGDMA utilized. Crosslinking density correlates with a decrease in swelling properties, while V_{2,s} correlates with an increase in swelling properties.

3.12. Swelling studies

The swelling ratios of hydrogels in different media were examined using different ratios of polymer, monomer and crosslinker (gelatin, AMPS, and EGDMA). Fig. 10A and B illustrate the dried hydrogels' physical appearance. Due to the hydrophilic nature of the polymers and monomers used in the preparation of hydrogels, the bonds between them begin to break when they are soaked in a variety of media. This results in the swelling of the hydrogels. Fig. 10C and D illustrate varia-

tions in the swelling rate of hydrogels with respect to pH (Jayaramudu et al., 2019). It was found that the swelling of the hydrogel was slightly higher at pH 1.2 and less at pH 7.4. Water in the environment caused the ionization of the hydroxyl (-OH) functional groups of the hydrogel, resulting in higher swelling. It was found that the swelling degree of hydrogel ranged between 21.75% and 60.84% at pH 1.2. The maximum percentage of the swelling degree of hydrogel was observed in GAE-6 at pH = 1.2 (60.84%), while the lowest percentage was found in GAE-3 at pH = 1.2 (21.75%). The percentage of the swelling degree of the hydrogel at pH = 7.4 was determined to be between 15.53% and 46.46%. GAE-6 had the highest swelling degree at pH = 7.4 (46.46%), and GAE-3 had the lowest swelling degree at pH = 7.4 (15.53%). Hydrogel swelling increased with the increase in gelatin ratio. The results of our study are in accordance with the findings of other researchers. A higher concentration of AMPS monomer will increase the equilibrium swelling degree of the hydrogel, given that AMPS contains

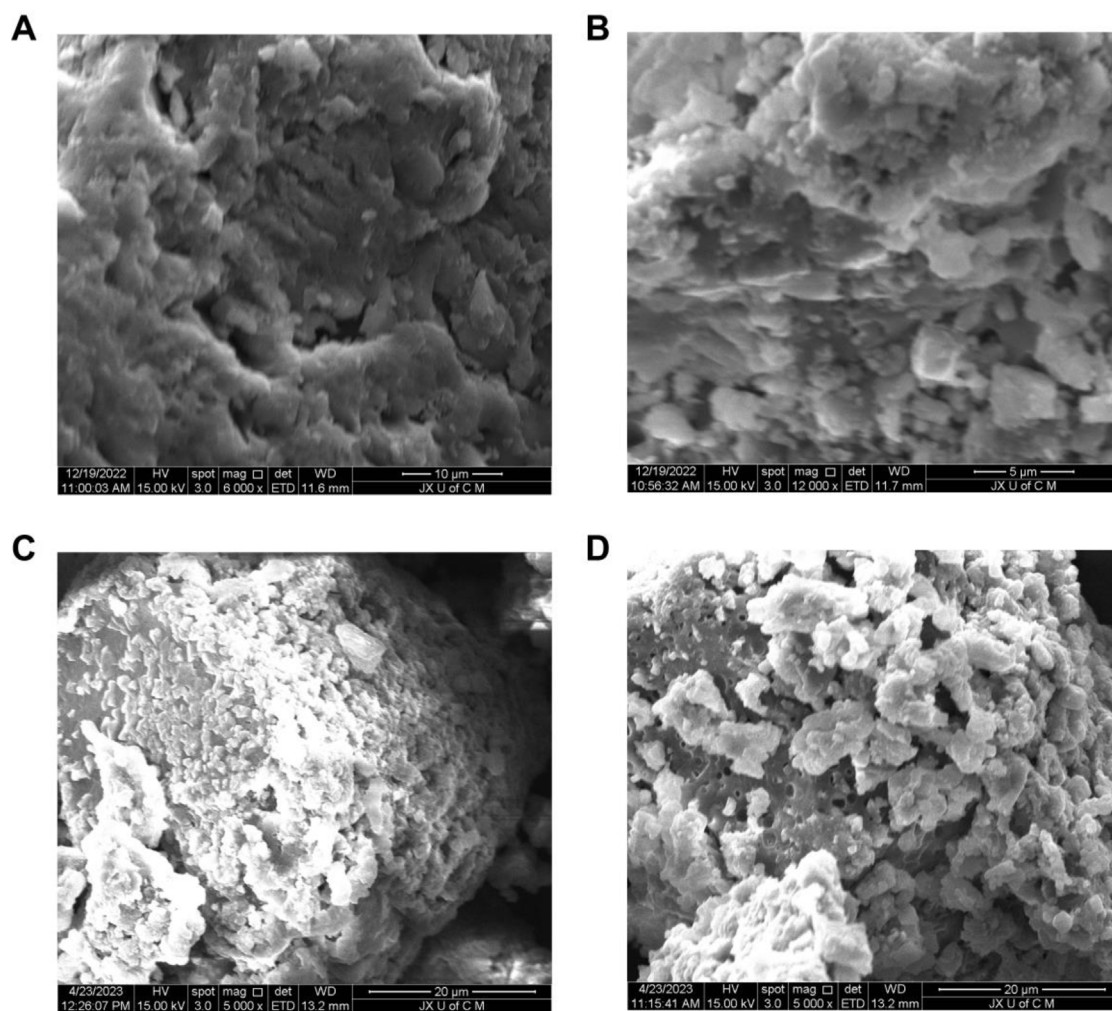


Fig. 7 Morphological characteristics of unloaded hydrogels at 6000 \times (A), 12000 \times (B) and TWHF-SD-loaded hydrogels at 5000 \times (C) and 5000 \times (D).

Table 3 The mechanical properties and drug loading of hydrogels.

F. Codes	Thickness (mm)	TS (N/m ²)	EAB (%)	Drug loaded per 1 g hydrogel (g)
GAE-1	1.25	0.518	49.3	0.512
GAE-2	1.68	0.842	60.1	0.335
GAE-3	1.08	0.978	71.4	0.296
GAE-4	0.99	0.668	66.5	0.317
GAE-5	1.68	0.842	60.1	0.335
GAE-6	1.39	0.389	36.9	0.602
GAE-7	1.28	0.466	51.3	0.448
GAE-8	1.68	0.842	60.1	0.335
GAE-9	1.26	0.695	63.3	0.543

abundant $-\text{CONH}_2$ and $-\text{SO}_3\text{OH}$ groups. The more of these groups present, the more likely they are to bind to water molecules, which are highly absorbent, so the more of these groups present, the higher the degree of absorption. AMPS improves the crosslinking density and storage modulus of hydrogel, enabling an optimal network structure to be formed. AMPS

content resulted in an increase in equilibrium swelling ratios and swelling rate constants for hydrogel, with more hydrogen bonds forming between water molecules and hydrogel, resulting in an increase in non-frozen and frozen bound water, thereby improving hydrogel water retention and improving swelling. Other researchers have also reported similar results

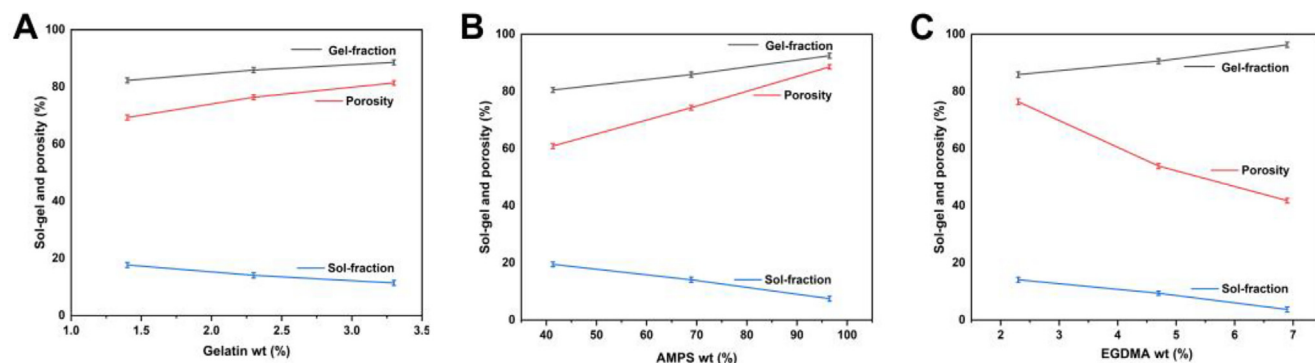


Fig. 8 Effect of gelatin (A), AMPS (B), and EGDMA (C) on sol-gel and porosity of hydrogel.

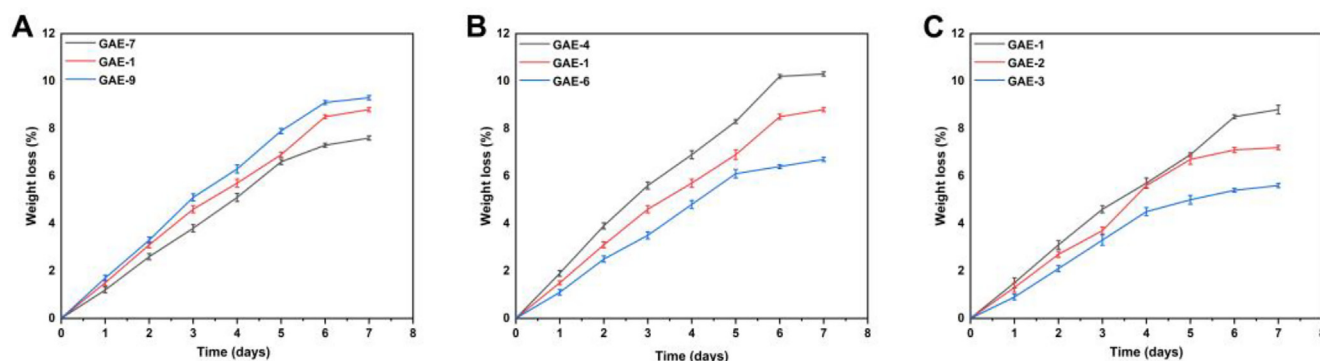


Fig. 9 Effect of gelatin (GAE-7,8,9) (A), AMPS (GAE-4,5,6) (B), and EGDMA (GAE-1,2,3) (C) on biodegradation of hydrogel.

Table 4 Flory-Huggins network parameters of Gelatin-g-AMPS hydrogels.

F. Codes	V _{2,s}	χ	M _c	M _r	N	D × 10 ⁻⁵ (cm ² sec ⁻¹)
GAE-1	0.037	0.512	4340.412	209.345	41.466	0.009
GAE-2	0.055	0.519	3621.621	209.069	34.645	0.013
GAE-3	0.064	0.522	3177.514	208.829	30.431	0.016
GAE-4	0.048	0.516	2456.521	206.923	23.743	0.012
GAE-5	0.055	0.519	3621.621	209.069	34.645	0.013
GAE-6	0.021	0.507	5408.163	208.689	51.829	0.005
GAE-7	0.041	0.514	1905.882	208.326	18.297	0.010
GAE-8	0.055	0.519	3621.621	209.069	34.645	0.013
GAE-9	0.029	0.509	3940.620	210.320	37.472	0.007

(Meng and Ye 2017). As the concentration of EGDMA increased, there was a decrease in swelling. When EGDMA concentration is increased in hydrogels, the packing density increases, and the porosity decreases. Thus, increased EGDMA concentration reduces water penetration into the hydrogel network, resulting in a decrease in swelling (Suhail et al., 2021).

3.13. Release and kinetic modelling analysis

The percentage of drug release in the buffer at pH of 1.2 ranged from 56.01% to 85.08%, as shown in Fig. 11. GAE-6 had the highest drug release rate at pH = 1.2 (85.08%), while

GAE-3 had the lowest drug release rate at pH = 1.2 (56.01%). The drug release rate was 50.02%–77.03% in the buffer with pH of 7.4. GAE-6 had the highest drug release (77.03%), while GAE-3 had the lowest drug release (50.02%). The release curve indicates that the release of TWHF was different in different pH buffers, with the maximum release occurring in pH buffer of 1.2. The maximum release rate was 85.08% after 48 h.

Water molecules diffuse into polymer networks when hydrogel discs are immersed in water. As a result of the diffusion of water, the hydrogel discs expand, causing channels to open, which in turn release the drug-loaded within them (Tabassum et al., 2022). Accordingly, we assessed the most appropriate model based on the regression coefficient value

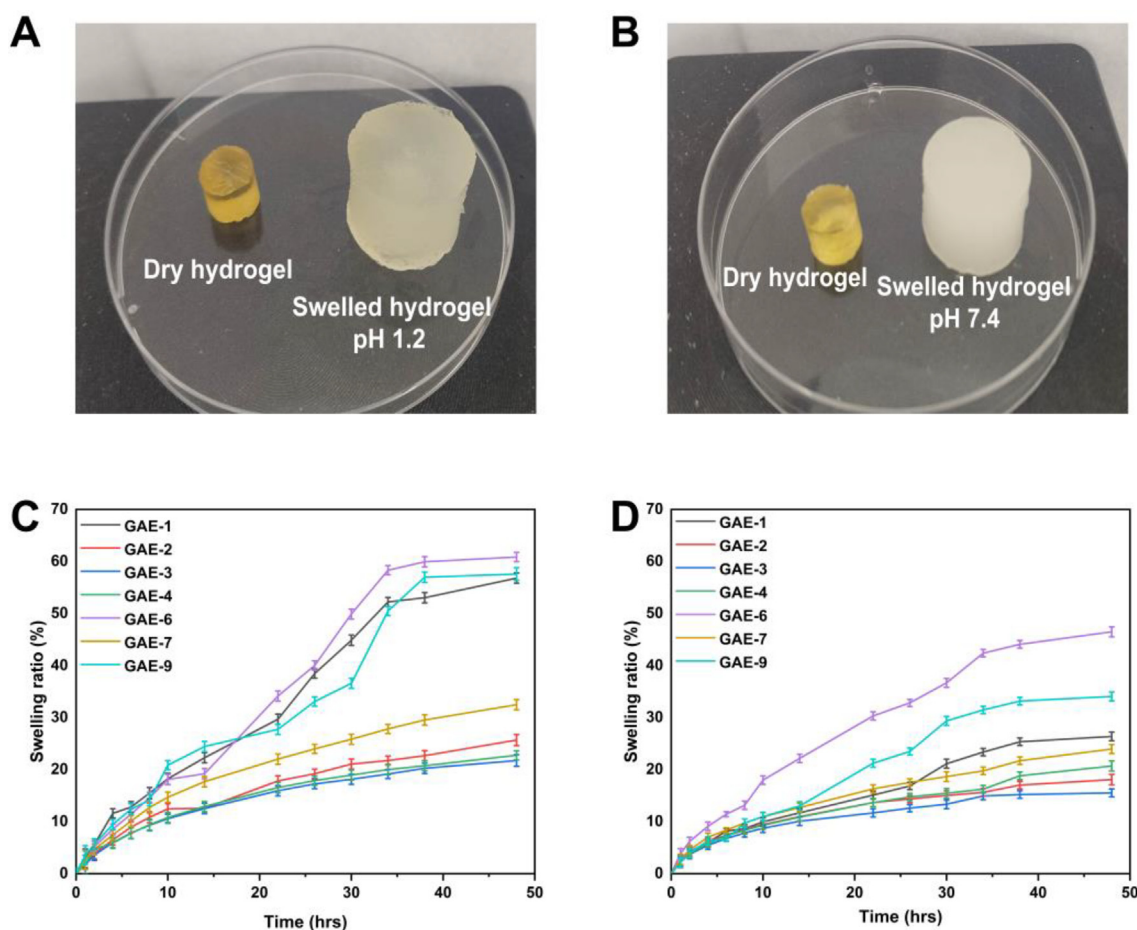


Fig. 10 The appearance of hydrogels after swelling at a pH of 1.2 (A) versus a pH of 7.4 (B). The swelling curves for hydrogels at 1.2 pH (C) and 7.4 pH (D) over time.

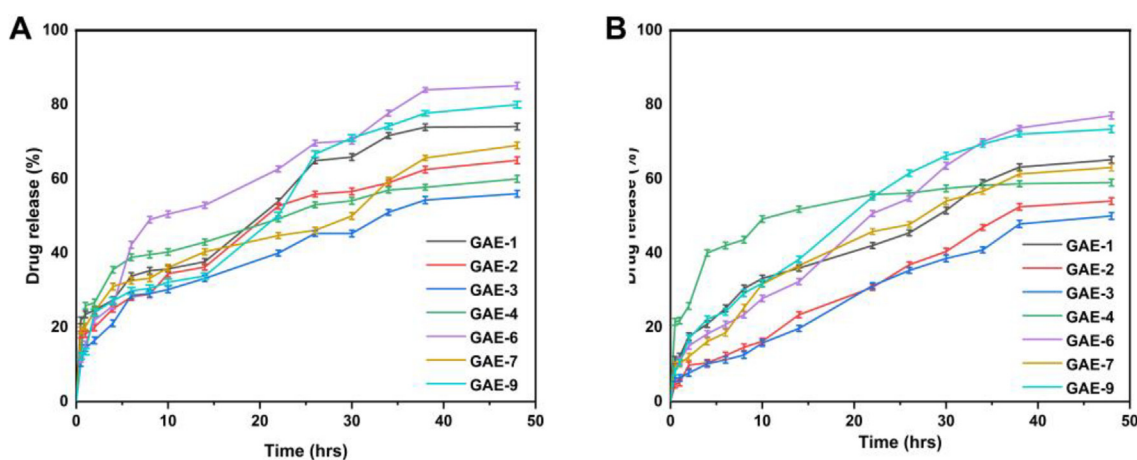


Fig. 11 The release of TWHF from hydrogels at pH 1.2 (A) and pH 7.4 (B) in 48 h.

close to 1 (Rashidi et al., 2022). A regression coefficient (r) was calculated for different concentrations of gelatin (GAE-7, GAE-8, GAE-9), which indicates that they follow Higuchi release kinetics as their regression coefficient values are closer to 1 than those of the Zero and First order models. Table 5 presents the regression coefficient values of samples (GAE-1,

GAE-2, GAE-3) containing various concentrations of the crosslinker EGDMA. Since the regression coefficients of these samples were close to 1, they also followed Higuchi's release kinetics. Additionally, regression coefficient (r) values for all samples (GAE-4, GAE-5, GAE-6) with varying concentrations of AMPS showed that drug release is controlled by diffusion.

Table 5 Release kinetics of TWHF-SD from Gelatin-g-AMPS hydrogel at pH 1.2 and 7.4.

F. Codes	pH	Zero Order		First Order		Higuchi Model		Korsmeyer-Peppas Model	
		K_0 (h ⁻¹)	r^2	K_1 (h ⁻¹)	r^2	K_2 (h ⁻¹)	r^2	r^2	n
GAE-1	1.2	1.392	0.9861	0.019	0.9927	7.639	0.9805	0.9923	0.750
	7.4	0.657	0.9822	0.008	0.9872	3.655	0.9876	0.9931	0.640
GAE-2	1.2	0.655	0.9603	0.008	0.9705	3.707	0.9961	0.9958	0.538
	7.4	0.483	0.9447	0.005	0.9534	2.778	0.9967	0.9985	0.544
GAE-3	1.2	0.575	0.9541	0.007	0.9644	3.268	0.9967	0.9964	0.517
	7.4	0.431	0.9361	0.005	0.9446	2.483	0.9933	0.9961	0.533
GAE-4	1.2	0.597	0.9574	0.007	0.9677	3.387	0.9970	0.9968	0.520
	7.4	0.515	0.9666	0.006	0.9729	2.918	0.9978	0.9978	0.516
GAE-5	1.2	0.655	0.9603	0.008	0.9705	3.707	0.9961	0.9958	0.538
	7.4	0.483	0.9447	0.005	0.9534	2.778	0.9967	0.9985	0.544
GAE-6	1.2	1.511	0.9841	0.021	0.9892	8.206	0.9696	0.9975	0.836
	7.4	1.177	0.9817	0.015	0.9940	6.532	0.9906	0.9959	0.665
GAE-7	1.2	0.828	0.9675	0.010	0.9799	4.667	0.9979	0.9980	0.562
	7.4	0.607	0.9662	0.007	0.9745	3.443	0.9994	0.9994	0.512
GAE-8	1.2	0.655	0.9603	0.008	0.9705	3.707	0.9961	0.9958	0.538
	7.4	0.483	0.9447	0.005	0.9534	2.778	0.9967	0.9985	0.544
GAE-9	1.2	1.315	0.9898	0.018	0.9877	7.160	0.9698	0.9903	0.823
	7.4	0.863	0.9830	0.010	0.9905	4.741	0.9799	0.9909	0.744

According to the Korsmeyer-Peppas model, controlled drug delivery devices usually show two types of diffusion: Fickian and non-Fickian. The Fickian diffusion mechanism occurs when the “ n ” value is $0.45 < n < 0.50$ for the cylindrical form of a controlled release device. As all the hydrogel formulations were used in cylindrical form, the hydrogels showed non-Fickian diffusion because the “ n ” values of all formulations ranged from 0.750 to 0.836.

3.14. Assessment of antioxidant potential

ABTS and DPPH were used as scavenging agents to evaluate the antioxidant activity of hydrogels, as shown in Fig. 12. Four formulations (GAE-6, GAE-9, GAE-1, and GAE-7) displayed higher antioxidant activity than the others. All of these formulations showed higher swelling and release. The percentage of antioxidant activity determined by DPPH ranged from 48.6% to 73.3%, of which GAE-6 had the highest antioxidant activity of 73.3%. The percentage of antioxidant activity measured by ABTS ranged from 42.8% to 71.2%, with GAE-6 having the maximum antioxidant activity of 71.2%. Celastrol, for instance, is one of the primary active ingredients in TWHF, and it is an antioxidant, anti-inflammatory, and anti-cancer compound (Li et al., 2017). Gelatin is a collagen derivative that absorbs water well (Nicholas et al., 2016). Our experiments showed that antioxidant properties were enhanced with gradual increases in gelatin content. Other studies have shown that the use of an adhesive film containing gelatin increases the antioxidant capacity of the film (Liu et al., 2015). We found that TWHF-SD-loaded hydrogels exhibited strong antioxidant properties depending on their proportions.

3.15. Evaluation of antimicrobial activity

Fig. 13 illustrates the zone of inhibition for Gram-positive (*E. coli* and *S. aureus*) and Gram-negative (*P. aeruginosa*) bacteria. In the negative control and blank hydrogel groups, no

zones were observed, whereas clear zones were observed in the positive control hydrogel (32 mm, 33 mm, and 35 mm) and TWHF-SD-loaded hydrogel (19 mm, 24 mm, and 27 mm), respectively, against *S. aureus*, *P. aeruginosa*, and *E. coli*. Accordingly, the percent bacterial inhibition rates of the TWHF-loaded hydrogels against *S. aureus*, *P. aeruginosa*, and *E. coli* were 59.37%, 72.72% and 77.14%, respectively. Antibiotics like cefepime have been proven to be effective against both Gram-positive and Gram-negative bacteria. During the testing of cefepime against selected bacteria strains, a smaller antibacterial zone was observed for Gram-negative bacteria than for Gram-positive bacteria. The structure of the bacteria’s cell wall may be responsible for this behaviour. Gram-negative bacteria have an outer membrane, an inner membrane, and a peptidoglycan wall (Kamaci and Kaya 2018). In contrast to Gram-negative bacteria, Gram-positive bacteria lack an outermost membrane, even though their cell walls are thick. Gram-negative bacteria’s outer membrane protects them from the outside environment. Consequently, Gram-positive bacteria have a larger inhibitory zone, allowing the tested compound to exert a greater antibacterial effect (Liu et al., 2022, Liu et al., 2023a, 2023b).

4. Conclusion

In this study, we prepared an amorphous solid dispersion of TWHF and analyzed it using UHPLC-Q-TOF-MS, which revealed 48 components. These include sesquiterpene alkaloids, diterpenes, and triterpene compounds. Additionally, a controlled-release hydrogel delivery system for TWHF-SD was fabricated using the free radical polymerization technique by grafting 2-acrylamido-2-methylpropane sulfonic acid (AMPS) onto the gelatin backbone. FTIR, XRD, TGA, and DSC analyses confirmed the formation of hydrogel networks and the successful loading of TWHF-SD, while SEM examination demonstrated the porous nature of these hydrogel networks. A slightly higher swelling of the hydrogels was

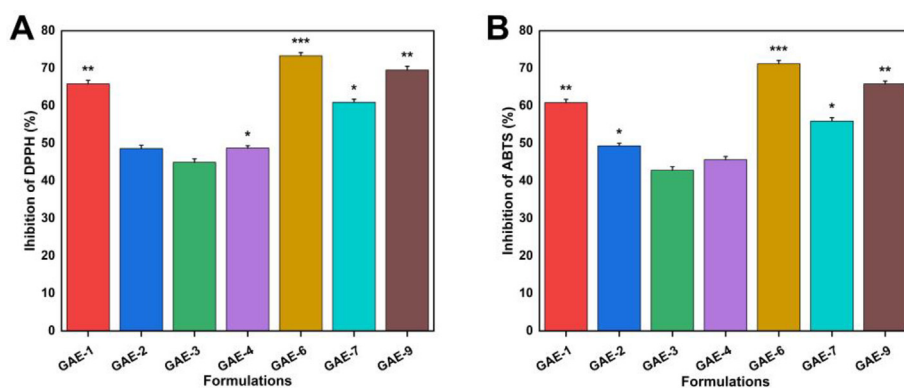


Fig. 12 Antioxidant properties of hydrogels as measured against DPPH (A) and ABTS (B).

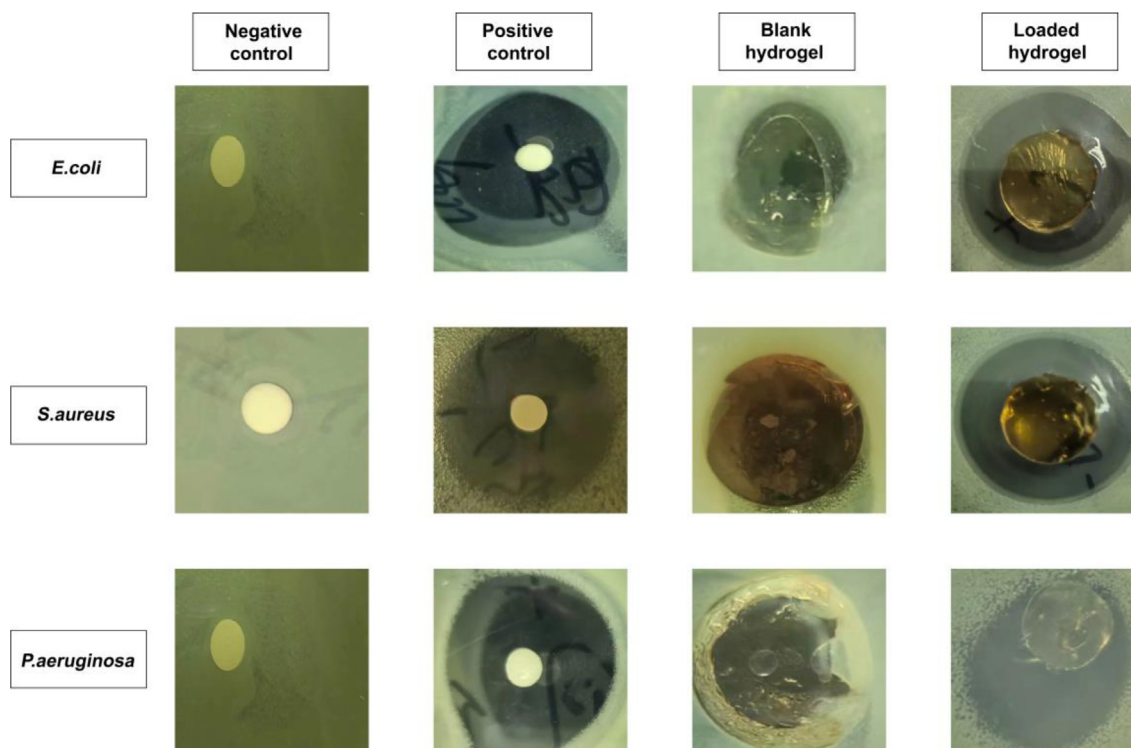


Fig. 13 The zones of inhibition against *E. coli*, *S. aureus*, and *P. aeruginosa* of negative control, positive control (cefepime), blank and TWHF-SD-loaded hydrogels.

observed at pH 1.2 (60.84% swelling) as compared to pH 7.4 (46.46% swelling). In addition, the synthesized hydrogels released the drug at a slightly higher rate after 48 h at pH 1.2 (85.08%) than at pH 7.4 (77.03%), with non-Fickian diffusion dominating the release mechanism. The drug release times and mechanical properties were improved when polymer ratios and monomer concentrations were increased. Furthermore, the hydrogels were found to be highly porous (91.62% porosity) and biodegradable (9.3% weight loss after seven days). Furthermore, the developed hydrogels demonstrated significant antioxidant activity in both DPPH and ABTS assays (inhibition by 73.3% and 71.2%, respectively). Additionally, the hydrogels exhibited excellent antibacterial properties against Gram-positive bacteria, including *E. coli* (zone of inhibition of 27 mm) and *S. aureus* (zone of inhibition of 19 mm), and Gram-negative bacteria, such as *P. aeruginosa* (zone of inhibi-

tion of 24 mm). In summary, Gelatin-g-AMPS hydrogels offer an intriguing alternative to conventional dosage forms for the extended delivery of solid dispersions of medicinal plants and hydrophilic drugs.

Funding

This study was supported by Jiangxi University of Traditional Chinese Medicine 1050 youth talent project (No. 5142001007), National Natural Science Foundation of China (No.82260756), Science and Technology Key Project of Jiangxi Provincial Department of Education (GJJ218915), and Jiangxi University of Chinese Medicine Science and Technology Innovation Team Development Program (No. CXTD-22004).

CRedit authorship contribution statement

Abid Naeem: Supervision, Writing – review & editing, Writing – original draft, Data curation, Conceptualization, Methodology, Investigation. **Chengqun Yu:** Writing – original draft, Methodology, Investigation, Data curation. **Yali Liu:** Funding acquisition. **Yali Feng:** Data curation. **Fan Jinhui:** Data curation. **Yongmei Guan:** Funding acquisition, Visualization, Resources.

Declaration of Competing Interest

The authors declare that they have no known competing financial interests or personal relationships that could have appeared to influence the work reported in this paper.

References

- Abbasi, A.R., Sohail, M., Minhas, M.U., et al, 2020. Bioinspired sodium alginate based thermosensitive hydrogel membranes for accelerated wound healing. *Int. J. Biol. Macromol.* 155, 751–765.
- Aguilar-Méndez, M.Á., Espinosa-Solares, T., Guerrero-Toledo, F.d. M., et al, 2020. Synthesis and characterisation of magnetite nanoparticles using gelatin and starch as capping agents. *IET Nanobiotechnol.* 14, 94–97.
- Biswal, D., Anupriya, B., Uvanesh, K., et al, 2016. Effect of mechanical and electrical behavior of gelatin hydrogels on drug release and cell proliferation. *J. Mech. Behav. Biomed. Mater.* 53, 174–186.
- Chang, A., Ye, Z., Ye, Z., et al, 2022. Citric acid crosslinked sphinganolipid hydrogel films supported ciprofloxacin for potential wound dressing application. *Carbohydr. Polym.* 291, 119520.
- Chen, F., Li, T., Li, S., et al, 2014. Preparation and characterization of *Tripterygium wilfordii* multi-glycoside nanoparticle using supercritical anti-solvent process. *Int. J. Mol. Sci.* 15, 2695–2711.
- Cheng, F.-M., Chen, H.-X., Li, H.-D., 2020. Recent advances in tough and self-healing nanocomposite hydrogels for shape morphing and soft actuators. *Eur. Polym. J.* 124, 109448.
- Elblbesy, M.A., Hanafy, T.A., Kandil, B.A., 2020. Effect of gelatin concentration on the characterizations and hemocompatibility of polyvinyl alcohol–gelatin hydrogel. *Biomed. Mater. Eng.* 31, 225–234.
- Elfawal, M.A., Towler, M.J., Reich, N.G., et al, 2015. Dried whole-plant *Artemisia annua* slows evolution of malaria drug resistance and overcomes resistance to artemisinin. *PNAS* 112, 821–826.
- Fan, B., Zhao, X., Liu, Z., et al, 2022. Inter-component synergetic corrosion inhibition mechanism of *Passiflora edulis* Sims shell extract for mild steel in pickling solution: Experimental, DFT and reactive dynamics investigations. *Sustain. Chem. Pharm.* 29, <https://doi.org/10.1016/j.scp.2022.100821> 100821.
- Ghumman, S.A., Noreen, S., Hameed, H., et al, 2022. Synthesis of pH-Sensitive Cross-Linked Basil Seed Gum/Acrylic Acid Hydrogels by Free Radical Copolymerization Technique for Sustained Delivery of Captopril. *Gels.* 8, 291.
- Gu, L., Li, T., Song, X., et al, 2020. Preparation and characterization of methacrylated gelatin/bacterial cellulose composite hydrogels for cartilage tissue engineering. *Regener. Biomater.* 7, 195–202.
- Guan, Y., Yu, C., Zang, Z., et al, 2023. Chitosan/xanthan gum-based (Hydroxypropyl methylcellulose-co-2-Acrylamido-2-methylpropane sulfonic acid) interpenetrating hydrogels for controlled release of amorphous solid dispersion of bioactive constituents of *Pueraria lobata*. *Int. J. Biol. Macromol.* 224, 380–395.
- Hu, X., Li, D., Gao, C., 2011. Chemically cross-linked chitosan hydrogel loaded with gelatin for chondrocyte encapsulation. *Biotechnol. J.* 6, 1388–1396.
- Jacob, S., Nair, A.B., Shah, J., et al, 2021. Emerging role of hydrogels in drug delivery systems, tissue engineering and wound management. *Pharmaceutics.* 13, 357.
- Jalil, A., Khan, S., Naeem, F., et al, 2017. The structural, morphological and thermal properties of grafted pH-sensitive interpenetrating highly porous polymeric composites of sodium alginate/acrylic acid copolymers for controlled delivery of diclofenac potassium. *Des. Monomers Polym.* 20, 308–324.
- Jayaramudu, T., Ko, H.-U., Kim, H.C., et al, 2019. Swelling behavior of polyacrylamide–cellulose nanocrystal hydrogels: swelling kinetics, temperature, and pH effects. *Materials.* 12, 2080.
- Jozaghkar, M.R., Sepehrian Azar, A., Ziaee, F., 2022. Preparation, Characterization, and swelling study of N, N'-dimethylacrylamide/acrylic acid amphiphilic hydrogels in different conditions. *Polym. Bull.* 79, 5183–5195.
- Jürgenliemk, G., Nahrstedt, A., 2003. Dissolution, solubility and cooperativity of phenolic compounds from *Hypericum perforatum* L. in aqueous systems. *Die Pharmazie – Int. J. Pharm. Sci.* 58, 200–203.
- Kakkar, V., Narula, P., 2022. Role of molecularly imprinted hydrogels in drug delivery – a current perspective. *Int. J. Pharm.* 121883.
- Kamaci, M., Kaya, I., 2018. Melamine-based poly (azomethine) hydrogels: Mechanical, biodegradability, drug loading and antibacterial properties. *Eur. Polym. J.* 108, 107–115.
- Kesharwani, P., Bisht, A., Alexander, A., et al, 2021. Biomedical applications of hydrogels in drug delivery system: An update. *J. Drug Delivery Sci. Technol.* 66, 102914.
- Khan, F., Atif, M., Haseen, M., et al, 2022. Synthesis, classification and properties of hydrogels: their applications in drug delivery and agriculture. *J. Mater. Chem. B* 10, 170–203.
- Kocak, F.Z., Yar, M., Rehman, I.U., 2022. Hydroxyapatite-integrated, heparin-and glycerol-functionalized chitosan-based injectable hydrogels with improved mechanical and proangiogenic performance. *Int. J. Mol. Sci.* 23, 5370.
- Laffleur, F., Keckeis, V., 2020. Advances in drug delivery systems: Work in progress still needed? *Int. J. Pharm.* 590, 119912.
- Li, Z., Jiang, X., Huang, H., et al, 2022. Chitosan/zein films incorporated with essential oil nanoparticles and nanoemulsions: Similarities and differences. *Int. J. Biol. Macromol.* 208, 983–994.
- Li, J.-W.-H., Vederas, J.C., 2009. Drug discovery and natural products: end of an era or an endless frontier? *Science* 325, 161–165.
- Li, X., Wu, N., Zou, L., et al, 2017. Protective effect of celastrol on myocardial ischemia–reperfusion injury. *Anatol. J. Cardiol.* 18, 384.
- Lim, H.Y., Ong, P.S., Wang, L., et al, 2021. Celastrol in cancer therapy: Recent developments, challenges and prospects. *Cancer Lett.* 521, 252–267.
- Lin, N., Zhang, Y.-Q., Jiang, Q., et al, 2021. Clinical practice guideline for tripterygium glycosides/tripterygium wilfordii tablets in the treatment of rheumatoid arthritis. *Front. Pharmacol.* 11, 608703.
- Liu, H., Fan, B., Liu, Z., et al, 2022. Electronic effects on protective mechanism of electropolymerized coatings based on N-substituted aniline derivatives for mild steel in saline solution. *J. Ind. Eng. Chem.* 106, 297–310.
- Liu, Y., Fan, B., Xu, B., et al, 2023a. Ambient-stable polyethyleneimine functionalized Ti3C2Tx nanohybrid corrosion inhibitor for copper in alkaline electrolyte. *Mater. Lett.* 337, 133979.
- Liu, Z., Fan, B., Zhao, J., et al, 2023b. Benzothiazole derivatives-based supramolecular assemblies as efficient corrosion inhibitors for copper in artificial seawater: Formation, interfacial release and protective mechanisms. *Corros. Sci.* 212, 110957.
- Liu, D., Nikoo, M., Boran, G., et al, 2015. Collagen and gelatin. *Annu. Rev. Food Sci. Technol.* 6, 527–557.
- Liu, P., Zhang, J., Wang, Y., et al, 2021. The active compounds and therapeutic target of tripterygium wilfordii hook. f. in attenuating proteinuria in diabetic nephropathy: a review. *Front. Med. (Lausanne)* 8, <https://doi.org/10.3389/fmed.2021.747922> 747922.

- Lorz, L.R., Yoo, B.C., Kim, M.-Y., et al, 2019. Anti-wrinkling and anti-melanogenic effect of *Pradosia mutisii* methanol extract. *Int. J. Mol. Sci.* 20, 1043.
- Martínez-Serrano, R.D., Ugone, V., Porcu, P., et al, 2022. Novel porphyrin-containing hydrogels obtained by frontal polymerization: Synthesis, characterization and optical properties. *Polymer* 247, 124785.
- Meng, Y., Ye, L., 2017. Synthesis and swelling property of superabsorbent starch grafted with acrylic acid/2-acrylamido-2-methyl-1-propanesulfonic acid. *J. Sci. Food Agric.* 97, 3831–3840.
- Mushtaq, F., Raza, Z.A., Batool, S.R., et al, 2022. Preparation, properties, and applications of gelatin-based hydrogels (GHs) in the environmental, technological, and biomedical sectors. *Int. J. Biol. Macromol.*
- Naeem, A., Hu, P., Yang, M., et al, 2022a. Natural Products as Anticancer Agents: Current Status and Future Perspectives. *Molecules* 27, 8367.
- Naeem, A., Ming, Y., Pengyi, H., et al, 2022b. The fate of flavonoids after oral administration: a comprehensive overview of its bioavailability. *Crit. Rev. Food Sci. Nutr.* 62, 6169–6186.
- Naeem, A., Yu, C., Zhu, W., et al, 2022c. Gallic Acid-Loaded Sodium Alginate-Based (Polyvinyl Alcohol-Co-Acrylic Acid) Hydrogel Membranes for Cutaneous Wound Healing: Synthesis and Characterization. *Molecules* 27, 8397.
- Naeem, A., Yu, C., Zang, Z., et al, 2023. Synthesis and Evaluation of Rutin-Hydroxypropyl β -Cyclodextrin Inclusion Complexes Embedded in Xanthan Gum-Based (HPMC-g-AMPS) Hydrogels for Oral Controlled Drug Delivery. *Antioxidants* 12, 552.
- Nicholas, M.N., Jeschke, M.G., Amini-Nik, S., 2016. Cellularized bilayer pullulan-gelatin hydrogel for skin regeneration. *Tissue Eng. A* 22, 754–764.
- Qu, J., Liang, Y., Shi, M., et al, 2019. Biocompatible conductive hydrogels based on dextran and aniline trimer as electro-responsive drug delivery system for localized drug release. *Int. J. Biol. Macromol.* 140, 255–264.
- Rahman, M.S., Al-Saidi, G.S., Guizani, N., 2008. Thermal characterisation of gelatin extracted from yellowfin tuna skin and commercial mammalian gelatin. *Food Chem.* 108, 472–481.
- Rahman, H.S., Othman, H.H., Hammadi, N.I., et al, 2020. Novel drug delivery systems for loading of natural plant extracts and their biomedical applications. *Int. J. Nanomed.*, 2439–2483
- Rashidi, Z., Bagheri Marandi, G., Taghvay Nakhjiri, M., 2022. Carboxymethyl cellulose-based nanocomposite hydrogel grafted with vinyllic comonomers: synthesis, swelling behavior and drug delivery investigation. *J. Macromol. Sci. A* 59, 421–432.
- Salahuddin, B., Wang, S., Sangian, D., et al, 2021. Hybrid gelatin hydrogels in nanomedicine applications. *ACS Appl. Bio Mater.* 4, 2886–2906.
- Sheridan, H., Kopp, B., Krenn, L., et al, 2015. Traditional Chinese herbal medicine preparation: invoking the butterfly effect. *Science* 350, S64–S66.
- Shi, C., Tao, F., Cui, Y., 2018. New starch ester/gelatin based films: developed and physicochemical characterization. *Int. J. Biol. Macromol.* 109, 863–871.
- Singh, B., Singh, B., 2020. Graft copolymerization of polyvinylpyrrolidone onto *Azadirachta indica* gum polysaccharide in the presence of crosslinker to develop hydrogels for drug delivery applications. *Int. J. Biol. Macromol.* 159, 264–275.
- Sousa, H.R., Lima, I.S., Neris, L.M.L., et al, 2023. Innovative hydrogels made from babassu mesocarp for technological application in agriculture. *J. Mol. Liq.* p. 121463.
- Suhail, M., Shih, C.-M., Liu, J.-Y., et al, 2021. Synthesis, Characterization, In-Vitro and In-Vivo Evaluation of Ketorolac Tromethamine-Loaded Hydrogels of Glutamic Acid as Controlled Release Carrier. *Polymers* 13, 3541.
- Sun, R., Dai, J., Ling, M., et al, 2022. Delivery of triptolide: a combination of traditional Chinese medicine and nanomedicine. *J. Nanobiotechnol.* 20, 194. <https://doi.org/10.1186/s12951-022-01389-7>.
- Sun, M., Zhao, L., Wang, K., et al, 2019. Rapid identification of “mad honey” from *Tripterygium wilfordii* Hook. f. and *Macleaya cordata* (Willd) R. Br using UHPLC/Q-TOF-MS. *Food Chem.* 294, 67–72.
- Tabassum, M., Pervaiz, F., Shoukat, H., 2022. Fabrication and evaluation of gelatin-PVA-co-poly (2-acrylamido-2-methylpropane sulfonic acid)-based hydrogels for extended-release of sitagliptin and metformin by employing response surface methodology. *Chem. Pap.* 76, 4081–4097.
- Tang, B., Liu, Z., Tian, Z., et al, 2019. Development and evaluation of synchronized and sustained release Tripterygium Wilfordii tablets based hot-melt extrusion and direct powder compression. *J. Drug Delivery Sci. Technol.* 53, 101208.
- Tang, B., Yang, X., Zhang, A., et al, 2022. Polypseudorotaxane hydrogel based on Tween 80 and α -cyclodextrin for sustained delivery of low molecular weight heparin. *Carbohydr. Polym.* 297, 120002.
- Tapdiqov, S., Tagiyev, D., Zeynalov, N., et al, 2022. Cumulative release kinetics of levothyroxine-Na pentahydrate from chitosan/arabinogalactane based pH sensitive hydrogel and its toxicology. *React. Funct. Polym.* 105334.
- Taylor, L.S., Zhang, G.G., 2016. Physical chemistry of supersaturated solutions and implications for oral absorption. *Adv. Drug Deliv. Rev.* 101, 122–142.
- Tchicailat-Landou, M., Petit, J., Gaiani, C., et al, 2018. Ethnobotanical study of medicinal plants used by traditional healers for the treatment of oxidative stress-related diseases in the Congo Basin. *J. Herbal Med.* 13, 76–90.
- Tong, L., Zhao, Q., Datan, E., et al, 2021. Triptolide: reflections on two decades of research and prospects for the future. *Nat. Prod. Rep.* 38, 843–860.
- Tytgat, L., Vagenende, M., Declercq, H., et al, 2018. Synergistic effect of κ -carrageenan and gelatin blends towards adipose tissue engineering. *Carbohydr. Polym.* 189, 1–9.
- Ullah, K., Khan, S.A., Murtaza, G., et al, 2019. Gelatin-based hydrogels as potential biomaterials for colonic delivery of oxaliplatin. *Int. J. Pharm.* 556, 236–245.
- Vigata, M., Meinert, C., Hutmacher, D.W., et al, 2020. Hydrogels as drug delivery systems: A review of current characterization and evaluation techniques. *Pharmaceutics* 12, 1188.
- Weathers, P.J., Arsenault, P.R., Covello, P.S., et al, 2011. Artemisinin production in *Artemisia annua*: studies in planta and results of a novel delivery method for treating malaria and other neglected diseases. *Phytochem. Rev.* 10, 173–183.
- Williams, H.D., Trevaskis, N.L., Charman, S.A., et al, 2013. Strategies to address low drug solubility in discovery and development. *Pharmacol. Rev.* 65, 315–499.
- Xu, Z., Liu, G., Li, Q., et al, 2022. A novel hydrogel with glucose-responsive hyperglycemia regulation and antioxidant activity for enhanced diabetic wound repair. *Nano Res.*, 1–11
- Yu, C., Chen, X., Zhu, W., et al, 2022. Synthesis of gallic acid-loaded chitosan-grafted-2-acrylamido-2-methylpropane sulfonic acid hydrogels for oral controlled drug delivery: in vitro biodegradation, antioxidant, and antibacterial effects. *Gels* 8, 806.
- Zang, Z., Zhao, S., Yang, M., et al, 2022. Blood chemical components analysis of honeysuckle and formulation of xanthan gum/starch-based (PVA-co-AA) hydrogels for controlled release. *Arab. J. Chem.* 15, 104312.
- Zhang, Y., Mao, X., Li, W., et al, 2021. *Tripterygium wilfordii*: an inspiring resource for rheumatoid arthritis treatment. *Med. Res. Rev.* 41, 1337–1374.
- Zhao, Q., Luan, X., Zheng, M., et al, 2020. Synergistic mechanisms of constituents in herbal extracts during intestinal absorption: focus on natural occurring nanoparticles. *Pharmaceutics* 12, 128.